Pramana – J. Phys. (2020) 94:154
https://doi.org/10.1007/s12043-020-02011-x

The neutron halo structure of ^{14}B, ^{22}N, ^{23}O and ^{24}F nuclei studied via the generalised Woods–Saxon potential

AHMED N ABDULLAH

Department of Physics, College of Science, University of Baghdad, Baghdad, Iraq
E-mail: Ahmednajim@scbaghdad.edu.iq

MS received 2 April 2020; revised 24 May 2020; accepted 6 July 2020

Abstract. The radial wave functions of the generalised Woods–Saxon (GWS) potential within the two-body model of (Core + n) have been used to study the ground-state density distributions of protons, neutrons and matter and the associated root mean square (rms) radii of neutron-rich ^{14}B, ^{22}N, ^{23}O and ^{24}F halo nuclei. The calculated results show that the radial wave functions of the generalised Woods–Saxon potential within the two-body model succeed in reproducing neutron halo in these exotic nuclei. Elastic electron scattering form factors for these nuclei are studied by combining the charge density distributions with the plane-wave Born approximation (PWBA).

Keywords. Generalised Woods–Saxon potential; two-body model; one-neutron halo nuclei.

PACS Nos 21.10.Gv; 25.30.Bf

1. Introduction

The development of experiments using radioactive nuclear beams allowed us to study nuclei far from the valley of stability, which led to the discovery of halo phenomena [1,2]. Halo phenomenon is a quantum effect arises as a result of the combined impact of small binding energy of the valence particle(s) and their low angular momentum ($l = 0, 1$) [3]. The experiments with exotic (halo) nuclei are challenging because specific techniques are required due to the low intensity with which the nuclei are produced and their short lifetime. It is impossible to make short-lived nuclei as targets. Therefore, the experiments must be performed in inverse kinematics. In this case a beam of radioactive nuclei is produced and it interacts with a stable target [4].

The charge and nuclear matter distributions as well as the root mean square (rms) radii of nuclear matter give important insights on nuclear wave functions and nuclear potentials. The matter density distributions and radii of the halo nuclei have been studied by measuring the reaction and interaction cross-sections. The relation between the nuclear density distribution and the total reaction cross-section is studied using the Glauber model [5].

Abdullah [6] has investigated ground-state properties such as the binding energy per nucleon, the ground-state densities and the corresponding rms radii of two-neutron ^{6}He, ^{11}Li, ^{12}Be and ^{14}Be halo nuclei using MSK7 parameter within the Skyrme–Hartree–Fock (SHF) method. Tanaka *et al* [7] have used Glauber-type calculation to measure the reaction cross-sections for ^{14}B and ^{8}He on proton target. They have also deduced the nucleon density distributions and the rms proton, neutron and matter radii of these nuclei. Each radius was consistent with some of the several theoretical values and also with some of the other experimental values. Abdullah [8] has used the SKxs25 parameters within the SHF model to investigate the nuclear structure of ^{8}B, ^{17}Ne, ^{23}Al and ^{27}P halo nuclei. It was found that the SKxs25 parameters with this model is suitable for describing the nuclear structure of the above halo nuclei. Suzuki *et al* [9] studied the interaction cross-section (σ_{I}) for ^{17}B on a carbon target at 880 A MeV. The result for σ_{I} was 1118 ± 22 mb. They also studied the rms matter radii of ^{17}B using the Glauber model based on the few-body reaction model and optical limit approximation. Their results for these two different methods were 2.99 ± 0.09 and 2.90 ± 0.06 fm, respectively. Tanaka *et al* [10] have measured the reaction cross-sections for ^{13,14,15}B on Be, C, Al and proton targets using the Glauber model. They have also deduced the proton, neutron and nucleon density based on the Glauber-type calculation. The result suggests that there is a large tail in neutron density distribution for ^{14}B, which can be referred to as

Published online: 24 October 2020

a one-neutron halo. The rms proton, neutron and matter radii for ^{13,14,15}B were also derived. Abdullah [11] has used the two-body model of (Core+n) within the radial wave functions of the cosh potential to investigate the ground-state features such as the proton, neutron and matter densities, the rms nuclear proton, neutron, charge and mass radii of unstable neutron-rich ^{14}B, ^{15}C, ^{19}C and ^{22}N nuclei. The calculated results show that the two-body model with the radial wave functions of the cosh potential succeeds in reproducing neutron halo in these nuclei.

In this study, we shall adopt the radial wave functions of the generalised Woods–Saxon (GWS) potential within the two-body model of (Core + n) to study the ground-state density distributions of protons, neutrons and matter and the associated rms radii of neutron-rich ^{14}B, ^{22}N, ^{23}O and ^{24}F halo nuclei. Elastic electron scattering form factors for these nuclei will be studied by combining the charge density distributions with the plane-wave Born approximation (PWBA).

2. Theory

In the case of exotic (halo) nuclei, it is reasonable to parametrise the core and halo densities separately. Therefore, the ground-state matter density distribution for the halo nuclei can be written as [11]

$$\rho_m(r) = \rho_c(r) + \rho_v(r), \tag{1}$$

where $\rho_c(r)$ and $\rho_v(r)$ are the core and valence (halo) densities, respectively and expressed as [12]

$$\rho_c(r) = \frac{1}{4\pi}\sum_{n\ell j} X_c^{n\ell j}\left|R_{n\ell j}(r)\right|^2, \tag{2}$$

$$\rho_v(r) = \frac{1}{4\pi}X_v^{n\ell j}\left|R_{n\ell j}(r)\right|^2, \tag{3}$$

where $X_{c(v)}^{n\ell j}$ refers to the number of protons or neutrons in the sub-shell, $n\ell j$ and $R_{n\ell j}(r)$ are the radial wave functions of the GWS potential taken from the solution to radial part of the Schrödinger equation using the GWS.

The moving of valence neutron around the core can be described with the Schrödinger equation [13]

$$\frac{\mathrm{d}^2R_{n\ell j}(r)}{\mathrm{d}r^2} + \frac{2m}{\hbar^2} \times\left[\varepsilon_{n\ell j} - V(r) - \frac{\hbar^2}{2m}\frac{\ell(\ell+1)}{r^2}\right]R_{n\ell j}(r) = 0, \tag{4}$$

where m is the reduced mass of the core and single nucleon, $\varepsilon_{n\ell j}$ is the single-particle binding energy and $V(r)$ is the core potential which can be written as [13]

$$V(r) = V_0(r) + V_{\mathrm{so}}(r)\,\boldsymbol{L}.\boldsymbol{S} + V_{\mathrm{c}}(r). \tag{5}$$

$V_0(r)$ is the central potential which takes the form of the GWS potential [14–16]:

$$V_0(r) = -\frac{V_0}{1+\mathrm{e}^{(r-R_0)/a_0}} - \frac{W_0\mathrm{e}^{(r-R_0)/a_0}}{\left[1+\mathrm{e}^{(r-R_0)/a_0}\right]^2}, \tag{6}$$

where V_0 and W_0 ($0 < W_0 < 150$ MeV) are the depths of the potential well. The GWS potential is reduced to the standard Woods–Saxon form for $W_0 = 0$.

$V_{\mathrm{so}}(r)$ is the spin-orbit potential expressed as [17]:

$$V_{\mathrm{so}}(r) = V_{\mathrm{so}}\frac{1}{r}\left[\frac{\mathrm{d}}{\mathrm{d}r}\frac{1}{\left(1+\mathrm{e}^{(r-R_{\mathrm{so}})/a_{\mathrm{so}}}\right)}\right] \tag{7}$$

and $V_{\mathrm{c}}(r)$ is the Coulomb potential (for protons only) generated by a homogeneous charged sphere of radius R_c [18]:

$$V_{\mathrm{c}}(r) = \begin{cases} \dfrac{Ze^2}{r} & \text{for } r > R_c \\ \dfrac{Ze^2}{R_c}\left[\dfrac{3}{2} - \dfrac{r^2}{2R_c^2}\right] & \text{for } r \le R_c \end{cases} \tag{8}$$

and $V_{\mathrm{c}}(r) = 0$ for neutrons.

The radii R_0, R_{so} and R_c are usually expressed as [17]

$$R_i = r_i\,A^{1/3}, \tag{9}$$

where A is the mass number of the nucleus.

The matter density of eq. (1) can be written as [17]

$$\rho_m(r) = \rho^p(r) + \rho^n(r), \tag{10}$$

where $\rho^p(r)$ and $\rho^n(r)$ are the proton and neutron densities, respectively, written as [17]

$$\rho^p(r) = \rho_c^p(r) + \rho_v^p(r) \tag{11}$$

$$\rho^n(r) = \rho_c^n(r) + \rho_v^n(r). \tag{12}$$

Here $\rho_p^c(r)[\rho_n^c(r)]$ and $\rho_p^v(r)\,[\rho_n^v(r)]$ are the core and valence proton [neutron] densities, respectively.

From the proton density $\rho_p(r)$ and the intrinsic charge distribution f_p of one proton, we can obtain the charge distribution of the nucleus using the following folding relation [19]:

$$\rho_{ch}(r) = \int \rho_p(r)\,f_p\left(r'-r\right)\mathrm{d}r', \tag{13}$$

where f_p takes the Gaussian form as follows [20]:

Table 1. Some properties for the selected nuclei.

Halo nucleus	(J^π, T) [22]	Half-life $(\tau_{1/2})$ [22]	Core configuration	Halo neutron configuration
^{14}B	$2^-, 2$	12.5 ms	$\{(1s_{1/2})^4, (1p_{3/2})^7, (1p_{1/2})^2\}$	$2s_{1/2}$
^{22}N	$0^-, 4$	23 ms	$\{(1s_{1/2})^4, (1p_{3/2})^8, (1p_{1/2})^3, (1d_{5/2})^6\}$	$2s_{1/2}$
^{23}O	$1/2^+, 7/2$	97 ms	$\{(1s_{1/2})^4, (1p_{3/2})^8, (1p_{1/2})^4, (1d_{5/2})^6\}$	$2s_{1/2}$
^{24}F	$3^+, 3$	384 ms	$\{(1s_{1/2})^4, (1p_{3/2})^8, (1p_{1/2})^4, (1d_{5/2})^7\}$	$2s_{1/2}$

Table 2. The GWS parameters employed in the present calculations.

	$V_0 = W_0$ (MeV)						
	Proton	Neutron					
Nuclei		Core	Valence	V_{so} (MeV)	$a_0 = a_{so}$ (fm)	$r_0 = r_{so}$ (fm)	r_c (fm)
^{14}B	68.127	64.891	62.540	6.0	0.512	1.385	1.439
^{22}N	68.334	52.738	41.580	6.0	0.636	1.415	1.376
^{23}O	58.216	50.787	36.760	6.0	0.723	1.498	1.371
^{24}F	63.262	55.642	40.770	6.0	0.785	1.428	1.366
^{10}B	59.758	59.758		6.0	0.517	1.341	1.477
^{15}N	49.352	49.352		6.0	0.519	1.315	1.422
^{16}O	49.587	49.587		6.0	0.516	1.311	1.413
^{19}F	58.187	58.187		6.0	0.557	1.318	1.398

$$f_p(r)=\frac{1}{\left(\sqrt{\pi}a_p\right)^3}\mathrm{e}^{(-r^2/a_p^2)}. \tag{14}$$

The rms radii of the neutron, proton and charge distributions can be calculated by [19]:

$$r_g = \langle r_g^2\rangle^{1/2} = \left[\frac{\int r^2\rho_g(r)\mathrm{d}r}{\int \rho_g(r)\mathrm{d}r}\right]^{1/2}, \; g = n,\, p,\, ch. \tag{15}$$

The PWBA has been used to study the elastic electron scattering form factors from the considered nuclei. In PWBA, the charge form factor is the Fourier transform of charge density [21]:

$$F(q) = \frac{4\pi}{Z}\int_0^\infty \rho_{ch}(r)\, j_0(qr) r^2 \mathrm{d}r, \tag{16}$$

where $j_0(qr)$ is the zero-order spherical Bessel function and q is the momentum transfer from the incident electron to the target nucleus.

3. Results and discussion

The radial wave functions of the so-called GWS potential within the two-body model of (Core + n) have been used to study the ground-state density distributions of protons, neutrons, core and matter and the associated rms radii of one-neutron ^{14}B, ^{22}N, ^{23}O and ^{24}F halo nuclei. Elastic electron scattering form factors for these nuclei are studied by combining the charge density distributions with PWBA. The radial wave functions of the GWS potential are used to describe the core and halo densities.

We assumed that ^{14}B, ^{22}N, ^{23}O and ^{24}F have a structure of a core ^{13}B, ^{21}N, ^{22}O and ^{23}F plus valence (halo) neutron occupying the orbit $2s_{1/2}$. Some properties of these halo nuclei are summarised in table 1 [22]. The GWS parameters (V_0, W_0, V_{so}, r_0, r_{so}, a_0, a_{so} and r_c) are adjusted to reproduce the single-particle binding energies of ref. [23] and matter rms radii of halo nuclei. In our calculations, we assumed that $V_0 = W_0$ (where $0 < W_0 < 150$ MeV [15]). The GWS parameters employed in the present calculations for the nuclei under study are listed in table 2. The theoretical rms radii of proton, neutron, core and matter distributions of ^{14}B, ^{22}N, ^{23}O and ^{24}F are compared with the existing experimental data [24] and listed in tables 3 and 4 together with the available calculated results obtained from the relativistic mean field (RMF) method [25]. The present results are in a good agreement with the referred experimental radii within the error range more than the results of RMF method. Table 5 displays a comparison between the calculated results of the single-particle binding energies (ε) and those of the shell model NushellX@MSU code for the investigated nuclei.

Table 3. The calculated and experimental proton and neutron rms radii.

Nuclei	$\langle r_p^2\rangle_{\rm cal}^{1/2}$	$\langle r_n^2\rangle_{\rm cal}^{1/2}$	$\langle r_n^2\rangle_{\rm exp}^{1/2}$ [24]	$\langle r_{ch}^2\rangle_{\rm cal}^{1/2}$
^{14}B	2.16	2.74	2.61 ± 0.13	2.24
^{22}N	2.41	3.25	3.41 ± 0.16	2.45
^{23}O	2.62	3.35	3.58 ± 0.05	2.67
^{24}F	2.62	3.22	3.29 ± 0.09	2.68

Table 4. The calculated and experimental core and matter rms radii.

Nuclei	$\langle r_{\rm core}^2\rangle_{\rm cal}^{1/2}$	$\langle r_{\rm core}^2\rangle^{1/2}$ RMF [25]	$\langle r_{\rm core}^2\rangle_{\rm exp}^{1/2}$ [24]	$\langle r_m^2\rangle_{\rm cal}^{1/2}$	$\langle r_m^2\rangle^{1/2}$ RMF [25]	$\langle r_m^2\rangle_{\rm exp}^{1/2}$ [24]
^{14}B	2.22	2.51	2.41 ± 0.05	2.55	2.68	2.51 ± 0.09
^{22}N	2.77	2.87	2.75 ± 0.03	3.01	2.97	3.07 ± 0.13
^{23}O	2.90	2.92	2.88 ± 0.06	3.12	2.98	3.20 ± 0.04
^{24}F	2.80	2.85	2.79 ± 0.04	3.01	2.94	3.03 ± 0.06

Table 5. The calculated single-particle binding energies.

		Proton		Neutron	
Nuclei	$n\ell_j$	$\varepsilon_{\rm cal}$ (MeV)	ε (MeV) [23]	$\varepsilon_{\rm cal}$ (MeV)	ε (MeV) [23]
^{14}B	$1s_{1/2}$	−40.695	−40.695	−40.226	−40.226
	$1p_{3/2}$	−21.917	−21.917	−21.773	−21.773
	$1p_{1/2}$	–	–	−18.712	−18.712
	$2s_{1/2}$	–	–	−0.970	−0.970
^{22}N	$1s_{1/2}$	−45.267	−45.267	−34.719	−34.719
	$1p_{3/2}$	−30.191	−30.191	−21.185	−21.185
	$1p_{1/2}$	−28.349	−28.349	−19.202	−19.202
	$1d_{5/2}$	–	–	−7.349	−7.349
	$2s_{1/2}$	–	–	−0.645	−0.645
^{23}O	$1s_{1/2}$	−36.829	−36.829	−33.887	−33.887
	$1p_{3/2}$	−23.835	−23.835	−21.486	−21.486
	$1p_{1/2}$	−20.184	−20.184	−19.786	−19.786
	$1d_{5/2}$	–	–	−8.783	−8.783
	$2s_{1/2}$	–	–	−0.70	−0.70
^{24}F	$1s_{1/2}$	−38.273	−38.273	−35.850	−35.850
	$1p_{3/2}$	−24.059	−24.059	−22.288	−22.288
	$1p_{1/2}$	−22.216	−22.216	−20.407	−20.407
	$1d_{5/2}$	−9.656	−9.656	−8.711	−8.711
	$2s_{1/2}$	–	–	−0.985	−0.985

Figures 1a–1d show the dependence of the matter density distributions (in fm^{-3}) on r (in fm) for ^{14}B, ^{22}N, ^{23}O and ^{24}F, respectively. The red-dashed and blue distributions are the calculated results when $W_0 \neq 0$ (GWS) and $W_0 = 0$ (WS), respectively. The experimental matter densities (grey region) of ^{14}B [26], ^{22}N, ^{23}O and ^{24}F [27] are also plotted in these figures. It is obvious that the red-dashed distribution describes the experimental data better than the blue one.

Figures 2a–2d exhibit the calculated core (purple distributions), valence (blue distributions) and matter (red-dashed distributions) densities for ^{14}B, ^{22}N, ^{23}O and ^{24}F, respectively. One can see from these figures that a long tail is exhibited in the calculated matter density distributions for all nuclei under study which are consistent with the experimental results.

Figure 3 demonstrates the proton (purple curves), neutron (blue curves) and matter (red-dashed curves) densities for ^{14}B (figure 3a), ^{22}N (figure 3b), ^{23}O (figure 3c) and ^{24}F (figure 3d). As shown from these figures, the typical performance of the halo nuclei (i.e. long tail) is clearly shown in the neutron density distributions (blue curves). The calculated difference between the proton and neutron rms radii is

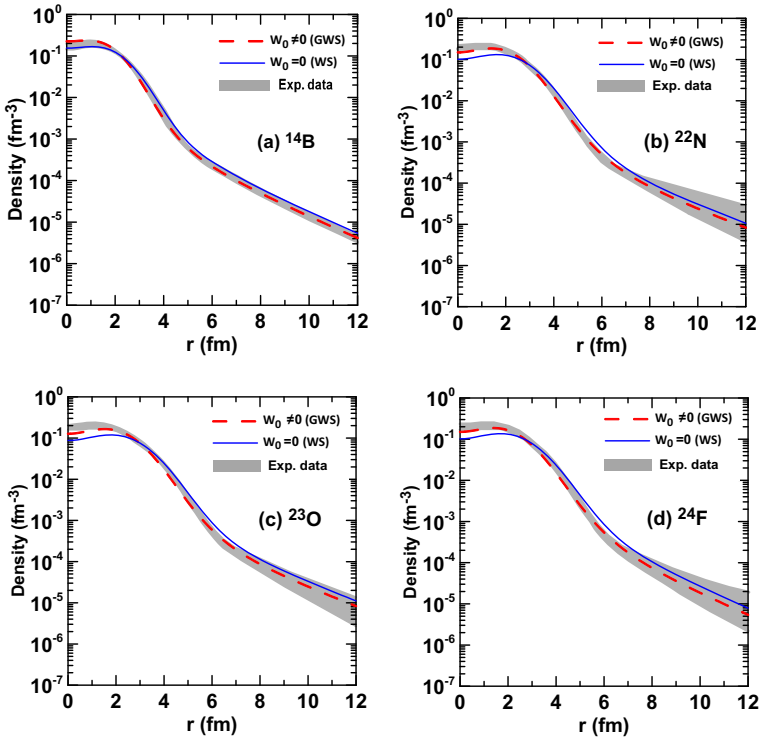

Figure 1. Matter density distributions of (**a**) ^{14}B, (**b**) ^{22}N, (**c**) ^{23}O and (**d**) ^{26}F halo nuclei.

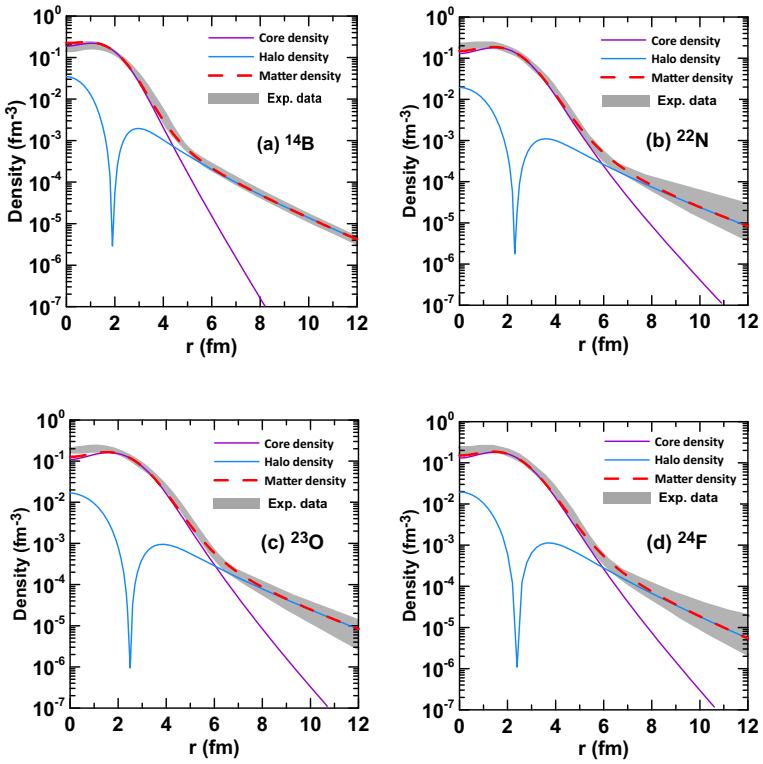

Figure 2. Core, halo and matter densities of (**a**) ^{14}B, (**b**) ^{22}N, (**c**) ^{23}O and (**d**) ^{26}F halo nuclei.

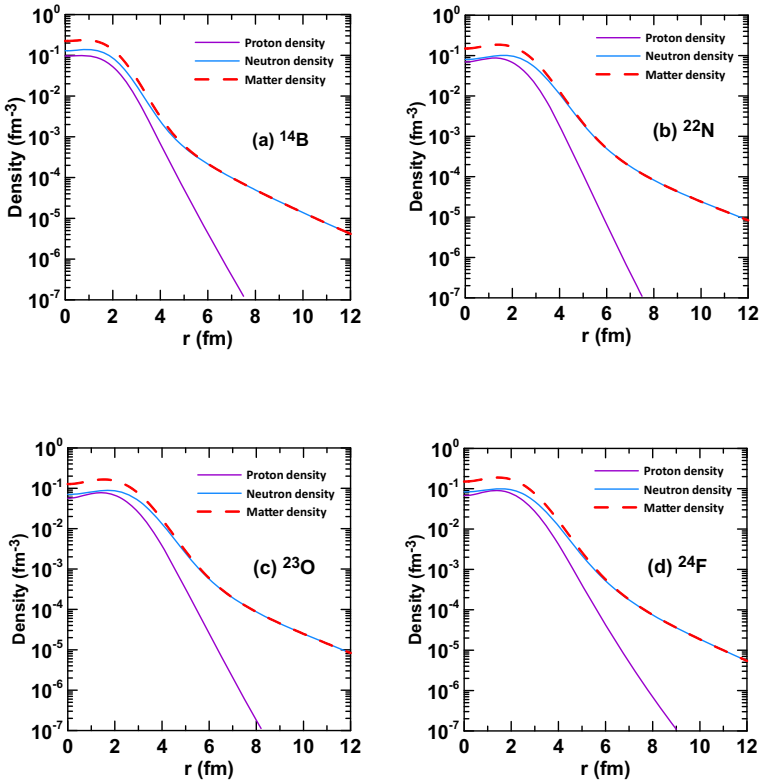

Figure 3. Calculated proton, neutron and matter densities for (**a**) ^{14}B, (**b**) ^{22}N, (**c**) ^{23}O and (**d**) ^{26}F halo nuclei.

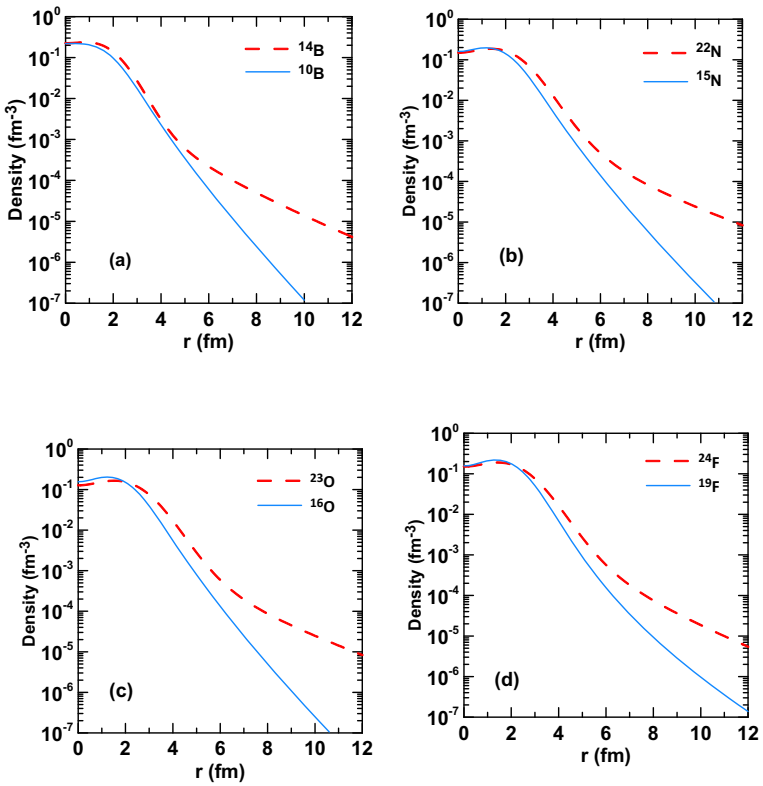

Figure 4. Calculated matter density distributions for isotope pairs ^{10,14}B, ^{15,22}N, ^{16,23}O and ^{19,24}F.

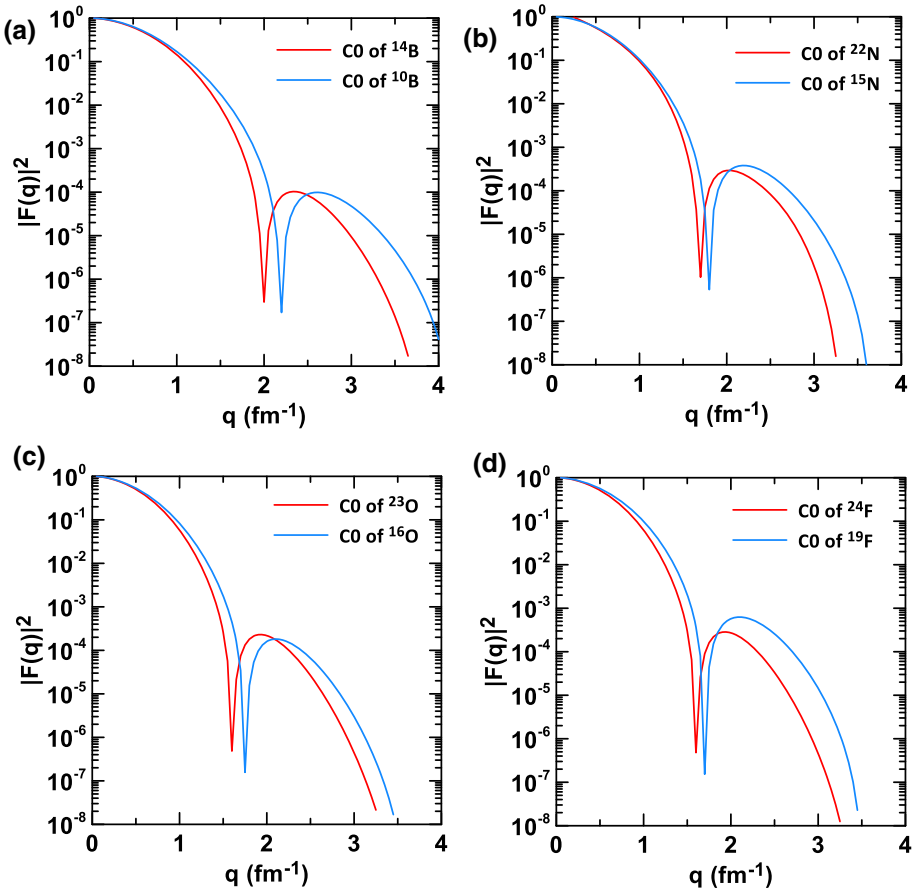

Figure 5. Elastic charge form factors for isotope pairs ^{10,14}B, ^{15,22}N, ^{16,23}O and ^{19,24}F.

$R_n - R_p = 0.58,\ 0.84,\ 0.73$ and 0.60 fm for ^{14}B, ^{22}N, ^{23}O and ^{24}F, respectively. This difference gives an extra support for the halo structure of these exotic nuclei.

Figures 4a–4d exemplify the calculated matter densities of ^{10,14}B, ^{15,22}N, ^{16,23}O and ^{19,24}F, respectively. The matter densities of unstable (^{14}B, ^{22}N, ^{23}O and ^{24}F) and stable (^{10}B, ^{15}N, ^{16}O and ^{19}F) nuclei are portrayed by the red-dashed and blue curves, respectively. From these figures it is obvious that, there is a long tail in the matter density distributions of the unstable nuclei due to the weak binding of the last neutron in these nuclei.

Figure 5 demonstrates the longitudinal $C0$ elastic electron scattering form factors for ^{10,14}B (figure 5a), ^{15,22}N (figure 5b), ^{16,23}O (figure 5c) and ^{19,24}F (figure 5d) calculated by PWBA. The red and blue curves refer to $C0$ of unstable (^{14}B, ^{22}N, ^{23}O and ^{24}F) and stable (^{10}B, ^{15}N, ^{16}O and ^{19}F) nuclei, respectively. In these figures each of the red curve and the blue curve has one diffraction maximum and one diffraction minimum throughout all the considered range of momentum transfer (q). Besides, the red curve has inward shift compared with the blue curve due to the contribution of the charge distribution of the neutrons themselves and also to the enhancement of the proton densities in the peripheral region.

4. Summary and conclusions

The radial wave functions of the so-called GWS potential within the two-body model of (Core + n) have been used to study the ground-state density distributions of protons, neutrons, core and matter and the associated rms radii of one-neutron ^{14}B, ^{22}N, ^{23}O and ^{24}F halo nuclei. The calculated results show that the radial wave functions of the GWS potential within the two-body model succeed in reproducing neutron halo in these exotic nuclei. From the calculated densities, it is found that ^{14}B, ^{22}N, ^{23}O and ^{24}F have a long tail in neutron and matter densities which is consistent with the experimental data. Elastic electron scattering form factors for these nuclei are studied by combining the charge density distributions with PWBA. It is found that the significant

difference between the charge form factors of the unstable nuclei (^{14}B, ^{22}N, ^{23}O and ^{24}F) and those of their stable isotopes (^{10}B, ^{15}N, ^{16}O and ^{19}F) is attributed to the contribution of the charge distribution of the neutrons themselves and also to the enhancement of the proton densities in the peripheral region.

References

[1] I Tanihata, H Hamagaki, O Hashimoto, S Nagamiya, Y Shida, N Yoshikawa, O Yamakawa, K Sugimoto, T Kobayashi, D E Greiner, N Takahashi and Y Nojiri, *Phys. Rev. Lett.* **55**, 2676 (1985)

[2] P G Hansen and B Jonson, *Europhys. Lett.* **4**, 409 (1987)

[3] W Zaijun and Z Z Ren, *Sci. China. Ser. G-Phys. Mech. Astron.* **47**, 42 (2004)

[4] S Ilieve, *Investigation of the nuclear matter density distributions of the exotic*^{12} *Be,* ^{14} *Be and* ^{8}*B nuclei by elastic proton scattering in inverse kinematics* (Johannes Gutenberg-University, 2008)

[5] I Tanihata, *J. Phys. G* **22**, 157 (1996)

[6] A N Abdullah, *Pramana – J. Phys.* **89**: 43 (2017)

[7] M Tanaka *et al*, *JPS Conf. Proc*. **6**, 020026 (2015)

[8] A N Abdullah, *Iran. J. Sci. Technol. Trans. Sci*. **44**, 283 (2020)

[9] T Suzuki *et al*, *Nucl. Phys. A* **658**, 313 (1999)

[10] M Tanaka *et al*, *Acta Phys. Polon. B* **48**, 461 (2017)

[11] A N Abdullah, *Int. J. Mod. Phys. E* **29**, 2050015 (2020)

[12] B A Brown, S E Massent and P E Hodgson, *J. Phys. G* **5**, 1655 (1979)

[13] W Meng *et al*, *Chin. Phys. C* **32**, 548 (2008)

[14] H Fakhri and J Sadeghi, *Mod. Phys. Lett. A* **19**, 615 (2004)

[15] C Berkdemir, A Berkdemir and R Sever, *Phys. Rev. C* **72**, 027001 (2005); *Phys. Rev. C* **74**, 039902(E) (2006)

[16] O Bayrak and E Aciksoz, *Phys. Scr*. **90**, 015302 (2015)

[17] A N Abdullah, *Int. J. Mod. Phys. E* **26**, 1750048 (2017)

[18] Y Chu, Z Z Ren and C Xu, *Eur. Phys. J. A* **37**, 361 (2008)

[19] L G Qiang, *J. Phys. G* **17**, 1 (1991)

[20] L R B Elton, *Nuclear sizes* (Oxford University Press, London, 1961) Chap. 2, Section 2.1.5, p 22

[21] A N Antonov, M K Gaidarov, D N Kadrev, P E Hodgson and E M D Guerr, *Int. J. Mod. Phys. E* **13**, 759 (2004)

[22] G Audi, F G Kondev, M Wang, W J Huang and S Naimi, *Chin. Phys. C* **41**, 030001 (2017)

[23] B A Brown and W D M Rae, *Nucl. Data Sheets* **120**, 115 (2014)

[24] S Ahmad, A A Usmani and Z A Khan, *Phys. Rev. C* **96**, 064602 (2017)

[25] J S Wang, W Q Shen, Z Y Zhu, J Feng, Z Y Guo, W L Zhan, G Q Xiao, X Z Cai, D Q Fang, H Y Zhang and Y G Ma, *Nucl. Phys. A* **691**, 618 (2001)

[26] M Fukuda *et al*, *EPJ Web Conf.* **66**, 02037 (2014)

[27] A Ozawa, *Eur. Phys. J. A* **13**, 163 (2002)